



are only a poor indicator for this; dollar values and variations of gross national product do not convey the amount of human suffering behind them. But they indicate the magnitude and importance of the task ahead, the development of a reliable forecast of year-to-year climate variations, of which ENSO variations are a major part.

### The Southern Oscillation

When Sir Gilbert Walker became Director-General of Observatories in the British colony of India in 1904 he set himself the task of trying to predict variations in the Indian monsoons and related droughts. To this end he started a project to examine global records of sea-level pressure, temperature, rainfall, and other variables from around the world. These records had been collected in the colonies of the major European powers and accumulated over some decades. Within each year of record, Walker calculated the seasonal averages for pressure and rainfall at each station. The averages would differ from year to year; but the patterns of the differences turned out to be similar over wide regions of the globe. An example is shown in Figure 19.2, which applies the technique of a twelve-month running mean to observations of air pressure at Darwin and of rainfall over the equatorial mid-Pacific Ocean (thus giving values for every month rather than seasonal values only, as in Walker's original method). The similarity in pattern comes out clearly.

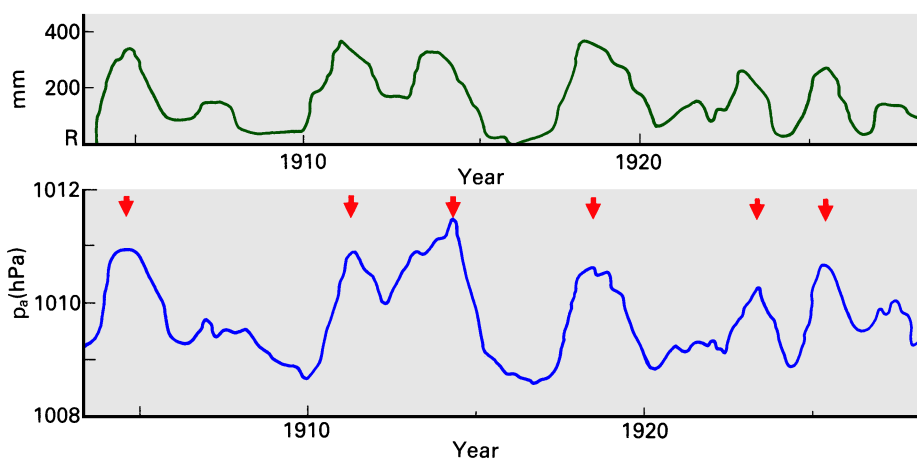


Fig. 19.2. Twelve-month running mean of air pressure  $p_a$  for Darwin (bottom) and of average rainfall  $R$  at a series of islands in the central equatorial Pacific Ocean between  $160^\circ\text{E}$  and  $150^\circ\text{W}$  (top). Arrows identify ENSO events for comparison with Fig. 19.4.

Walker plotted world maps of these differences and found that they were dominated by a single spatial pattern. Figure 19.3 shows a modern compilation of this spatial pattern, using objective mathematical methods. The "Southern Oscillation Index" used for the figure is a composite number derived from observations of air pressure at sea level for Cape



Town, Bombay, Djakarta, Darwin, Adelaide, Apia, Honolulu, and Santiago de Chile. (This is not the only definition of the Index in use; a more commonly used simpler version uses the difference in air pressure at sea level between Tahiti and Darwin). Its time history during the present century is given in Figure 19.4 (which, by comparison with Figure 19.2, shows that air pressure at Darwin contributes to the Southern Oscillation Index (SOI) in the inverse sense: Darwin air pressure is low when the SOI is high, and high when the SOI is low). The correlation map indicates a cellular structure of the air pressure field in the tropics, with high pressure in the central South Pacific Ocean and low air pressure over Australia, south-east Asia and India, central and southern Africa, and South America when the SOI is high. As the SOI reverses from positive to negative (as occurred, for example, from 1971 to 1972; see Figure 19.4), so does the spatial pattern, the highs turning into lows and the lows into highs. When searching for a name for the phenomenon, Walker compared it with the more regular seasonal variations of air pressure over the North Atlantic Ocean (the natural point of reference for a colonial officer of the British Empire) and chose the term "Southern Oscillation" for what is essentially a phenomenon of the tropics. His choice of name has now been accepted by meteorologists in both hemispheres.

## **El Niño**

One of the richest fishing regions of the World Ocean, the South Pacific coastal upwelling region along the coast of Peru, Chile, and Ecuador, occasionally experiences an influx of warm tropical water which suppresses the upwelling of nutrients. The *anchoveta*, which inhabit these waters in their millions forming the nutritional basis for a huge bird population and the stock for an important fish meal industry, depend on the supply of nutrients into the surface layer. They avoid the warm nutrient-poor water, which causes mass mortality amongst the birds (Figure 19.5). If the extent of the tropical influx is very severe, mass mortality can occur among the fish as well; hydrogen sulfide from decaying fish has been known to blacken the paint on ships in Callao harbour. The high temperatures along the South American coast last for about a year or more before conditions return to those which prevailed before the influx of tropical water.

The phenomenon has become known as El Niño, a term originally used by the fishermen of the Peruvian port of Paita to describe an influx of warm but nutrient-rich coastal water from the Gulf of Guayaquil (Tomczak, 1981b; Philander, 1990). This influx, which heralded good catches, usually occurs in December, which the fishermen (and millions of people in Christian communities around the world) associate with Christmas. The choice of "el niño" (the child) for an oceanic phenomenon as welcome and awaited as the birth of Christ appears sensible. Unfortunately, the influx of tropical nutrient-poor oceanic water associated with the suppression of the upwelling also manifests itself in a rise of surface temperature in December. When oceanographers began studying the phenomenon they failed to differentiate between the two different advective processes and adopted the local term El Niño for an oceanic phenomenon of much larger scale and of devastating effects for the fishermen.

Although oceanographers have been aware of the phenomenon for many decades (e.g. Sverdrup *et al.*, 1942), it was not until 1966 that Bjerknes (1966, 1969), a meteorologist who had become interested in ocean dynamics, pointed out the close relation



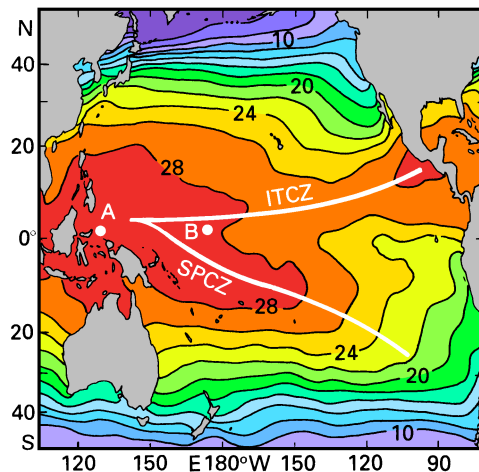


Fig. 19.7. The positions of the Intertropical Convergence Zone (ITCZ) and the South Pacific Convergence Zone (SPCZ) in relation to the annual mean sea surface temperature ( $^{\circ}\text{C}$ ), based on Levitus (1982). See text for the significance of locations A and B.

The combined process of El Niño and the Southern Oscillation has become known as ENSO, and the suppression of upwelling in the east accompanied by a drought in the west is now called an *ENSO event*. During the last two decades, with the availability of rainfall estimates over many years (derived from the outgoing long wave radiation measurements; see Chapter 18) and with improved knowledge of the SST distribution, it has become clear that ENSO is an instability of the coupled ocean - atmosphere system in the tropics. An indication of the effectiveness of the coupling can be seen with the intense rainfall bands of the ITCZ and SPCZ and the associated SST maxima; both are consistently found in close proximity. In an ENSO event, the entire Pacific air - sea system - rain bands and their associated winds, wind-driven currents and SST patterns - all move eastwards together, and the apex formed by the ITCZ and SPCZ in the west, which before the ENSO event was located at point A of Figure 19.7, moves to the dateline (point B). On average, the rainfall and SST maxima remain so close to one another that it is not possible to tell through the noise of shorter timescale rainfall variations whether the SST changes are causing the changes in rainfall or vice versa. The rainfall in the central Pacific Ocean strengthens, so that the convection system there competes successfully with the neighbouring convection systems for a while, suppressing their rainfall. Severe drought in Australia, Indonesia and to a lesser extent South Asia results. The centre of convection stays near the central equatorial Pacific Ocean (point B in Figure 19.7) for a year or more, before returning to the more common location in the far west (point A), bringing the ENSO event to an end. More detailed analysis of the time development of an ENSO event requires some elementary knowledge of tropical ocean dynamics, which we will introduce in the next few paragraphs.

### Some aspects of ENSO dynamics

Understanding the evolution of an ENSO event begins with an understanding of the evolution of the SST field. Many factors can influence the sea surface temperature. A change in wind speed affects evaporative heat loss; wind stresses create Ekman drifts, which advect surface water horizontally, and also create Ekman pumping, which changes the



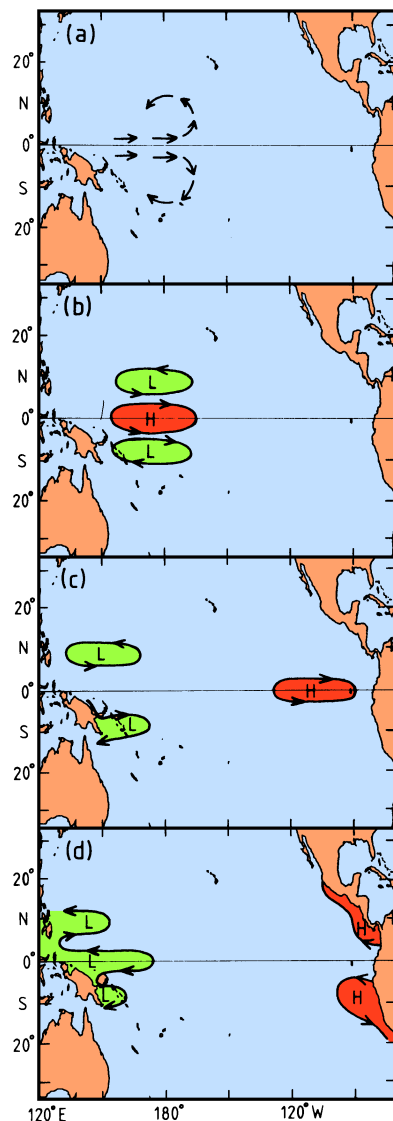


Fig. 19.9. Sketch of wave propagation during an ENSO event. (a) Wind stress anomalies associated with a typical westerly wind burst, (b) distribution of thermocline depth anomalies a few days after the westerly wind burst; Ekman convergence has piled thermocline water up near the equator, at the expense of off-equatorial regions, (c) distribution of thermocline depth anomalies about a month after a westerly wind burst; the off-equatorial regions of shallowed thermocline have moved slowly westward as Rossby waves, while the equatorial region of deepened thermocline has moved rapidly eastwards as an equatorial Kelvin wave, (d) distribution of thermocline depth anomalies about two months after a westerly wind burst; the Rossby waves have reached the western boundary, propagated equator-ward and created a new (upwelling) equatorial Kelvin wave emanating from the western boundary; the first equatorial Kelvin wave has reached the eastern boundary, spread poleward and created new Rossby waves that are starting to propagate slowly back into the Pacific Ocean.

The regions of shallowed thermocline near  $5-7^{\circ}\text{N}$  and  $5-7^{\circ}\text{S}$  at first move westward, by the Rossby wave propagation mechanism discussed in Chapter 3. It can be shown that eqn (3.11), which gave us the Rossby wave propagation speed as a function of latitude in a  $1\frac{1}{2}$  layer ocean, is no longer valid at these short distances from the equator; nevertheless, it gives a useful first approximation. For typical thermocline depths  $H$  of 150 m and a density ratio  $\Delta\rho/\rho = 0.004$  the shallow thermocline regions move west at  $6^{\circ}\text{N}$  or  $\text{S}$  at a speed of about  $0.3 \text{ m s}^{-1}$ , taking a few months to reach the western boundary, as sketched in Figure 19.9c.

Figure 19.9c shows also that the equatorial thermocline depression has moved rapidly eastward. This movement occurs at a speed of  $c_g = (g \Delta\rho H / \rho)^{1/2}$ , or about  $2.5 \text{ m s}^{-1}$ ,



The reflected Kelvin waves have longer period than the westerly wind burst that gave rise to them, and correspondingly lower amplitude. Meanwhile the first equatorial Kelvin wave has reached the east Pacific coast and propagated poleward as two coastal Kelvin waves. These in turn generate new - though diffuse - Rossby waves that radiate away from the eastern boundary (Figure 19.10b).

It can be imagined that these changes in thermocline depth induced by a westerly wind burst will affect SST in rather complex ways, far beyond the winds that produce them. The initial downwelling Kelvin waves of Figure 19.9b have two effects in the east Pacific Ocean. First they depress the thermocline, so that — even though upwelling favourable winds are still active — the upwelled water is substantially warmer than before. (This effect is not as strong in the central west Pacific Ocean, where the upwelled water is quite warm both before and during the passage of the Kelvin wave.) Secondly, the associated eastward currents point down the mean zonal SST gradient in the equatorial Pacific Ocean; i.e. horizontal advection also results in warming. As described in Chapter 18, Ekman drifts carry the warmer upwelled water poleward, so the effects on SST extend substantially further from the equator than the 300 km width of the original Kelvin wave. When the coastal Kelvin waves pass along the region of very shallow thermocline next to the Peru coast, they cause the increases in SST associated with an El Niño. The Rossby waves reflected off the eastern boundary in Figure 19.9c probably also play a role in SST change.

### **Anatomy of an ENSO event**

This very brief summary of equatorial dynamics and our qualitative understanding of the competition between tropical convection cells from the last chapter allows us to investigate the development of a typical ENSO event in some detail. Before entering the discussion it is useful to define some terms. The time history of the Southern Oscillation Index (Figure 19.4), which is low during ENSO events, tells us that ENSO years are significantly less frequent than non-ENSO years. Distributions of oceanic or atmospheric parameters drawn from long-term annual means (such as the SST map of Figure 19.7) therefore reflect conditions during non-ENSO years. Some scientific publications and many press and television reports therefore often refer to the non-ENSO situation as the "normal" situation. From the previous discussion it should be clear that ENSO events are not abnormalities; they are basic elements of the coupled ocean - atmosphere system. Labelling a particular set of years as normal is therefore not justified. This fact has become more and more accepted in recent years, and definitions such as non-ENSO mean, ENSO-mean, pre-ENSO mean, and post-ENSO mean have found more widespread use. They refer to average conditions during years with comparable SOI values. An ENSO-mean, for example, is computed from data for all years with an SOI minimum; the non-ENSO mean would then be computed from data for all remaining years. A pre-ENSO mean uses only data from years preceding ENSO years, while a post-ENSO mean results from data for years following ENSO years. More recently, years with unusually high SOI values, which represent a particularly strong "run" of the feedback loop when the centre of high SST is at point A of Figure 19.7, have become known as "La Niña" years (the girl, as opposed to the strict meaning of El Niño, the boy). Whether this term will become generally accepted remains to be seen.



is accompanied by high rainfall anomalies there; rainfall is below average at *B* (near Nauru, 170°E; Figure 19.11) at this time.

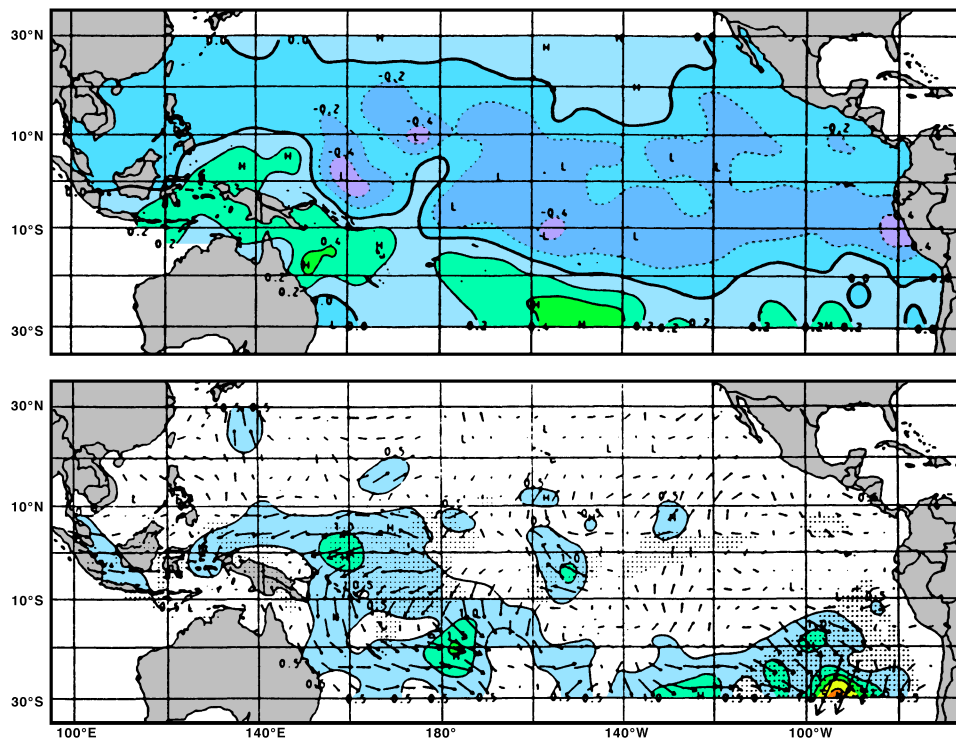


Fig. 19.12. SST anomaly ( $^{\circ}\text{C}$ ) and wind anomaly ( $\text{m s}^{-1}$ ), during the antecedent phase of ENSO (August - October preceding the ENSO year). The magnitude of the wind anomaly is indicated by arrow length and also contoured in  $0.5 \text{ m s}^{-1}$  intervals. Shading indicates regions where fewer than 10 observations were available in a  $2^{\circ}$  square. From Rasmusson and Carpenter (1982).

The onset phase, seen in Figure 19.13, corresponds to November - January preceding the ENSO event. The sun has crossed the equator, and the Australian summer monsoon has started. Wind anomalies have reversed in the equatorial western Pacific region and just north of Australia. Because the monsoon winds reverse seasonally, this in fact represents a strengthening of the Australian summer monsoon winds. This is not unusual, given that the preceding Asian summer monsoon was strong; a strong Asian monsoon is usually followed by a strong Australian monsoon (Meehl, 1987). The slight cooling of SST of about  $0.4^{\circ}\text{C}$  for the Indonesian region is probably due to excess evaporation, caused by the stronger than usual Australian monsoon winds. There is also a clear warming of about the same amount near  $170^{\circ}\text{E}$  (point *B* in Figure 19.7), and strong rainfall has started here (Figure 19.11). Rain has correspondingly decreased near *A*. Once again, inspection of Figure 19.7 shows that these small changes in SST imply substantial shifts of the



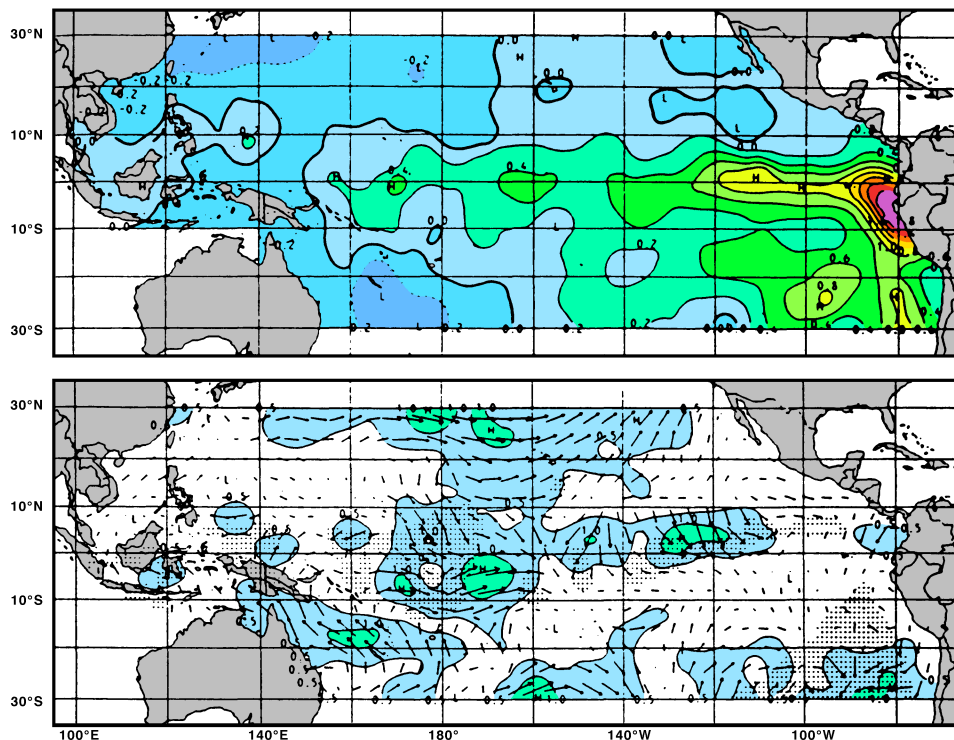


Fig. 19.14. SST anomaly ( $^{\circ}\text{C}$ ) and wind anomaly (m/s), during the peak phase of ENSO (March - May). For details see Fig. 19.12. From Rasmusson and Carpenter (1982).

The westerly wind anomalies in the western Pacific region of Figure 19.13 continue weakly into the peak phase of March - May, and they evidently drive downwelling equatorial Kelvin waves. The effect of these is evident in Figure 19.14; a marked warm SST anomaly has developed near South America. As explained in the preceding section, the Kelvin waves have a stronger effect on SST in the shallow thermocline of the east Pacific than in the central and west Pacific Ocean. In contrast, the small warming in the central Pacific Ocean in Figure 19.13 is probably largely due to horizontal advection.

On the basis of competition between convection centres, one might expect the centre near *B* of Figure 19.7 to “run away” after its formation. Curiously, however, this does not happen between November - January and March - May. Perhaps the reason is that the most active convection has moved with the SST to be well south of the equator during late southern summer, i.e. from February through April. The rainfall maximum near Nauru moves further east, to the Line Islands, during this period.

However, around May - June of an ENSO year when the Southern Hemisphere convection dies and a new Southwest Monsoon begins, drastic changes occur in the Pacific circulation (Figure 19.15). By August - October, violent westerly wind bursts are occurring, and SST increases throughout the east and central Pacific; the SST is reduced near Indonesia, and Indonesia and Australia experience their greatest drought intensity.



west Pacific Ocean. However, we are then confronted with a data quality problem. For example, the amount of heat needed to generate the  $0.4^{\circ}\text{C}$  warming in the top 50 m or so near *B* at the start of an ENSO event is only about  $10 \text{ W m}^{-2}$ . As was noted in the last chapter, the algorithms used to estimate heat fluxes currently have errors of substantially more than this. Hence improvement of heat flux algorithms has become a primary goal of ENSO research. It has already been shown that latent heat loss at low wind speeds has been seriously underestimated by some commonly used algorithms (Godfrey *et al.*, 1991) and that inclusion of low-wind evaporation in some atmospheric circulation models radically improves their representation of the monsoons. The mixing of cool water into the surface mixed layer is certainly crucial in the east Pacific and can also easily make significant contributions to SST change in the west Pacific Ocean, so improvement of mixing algorithms is also a high priority for ENSO research.

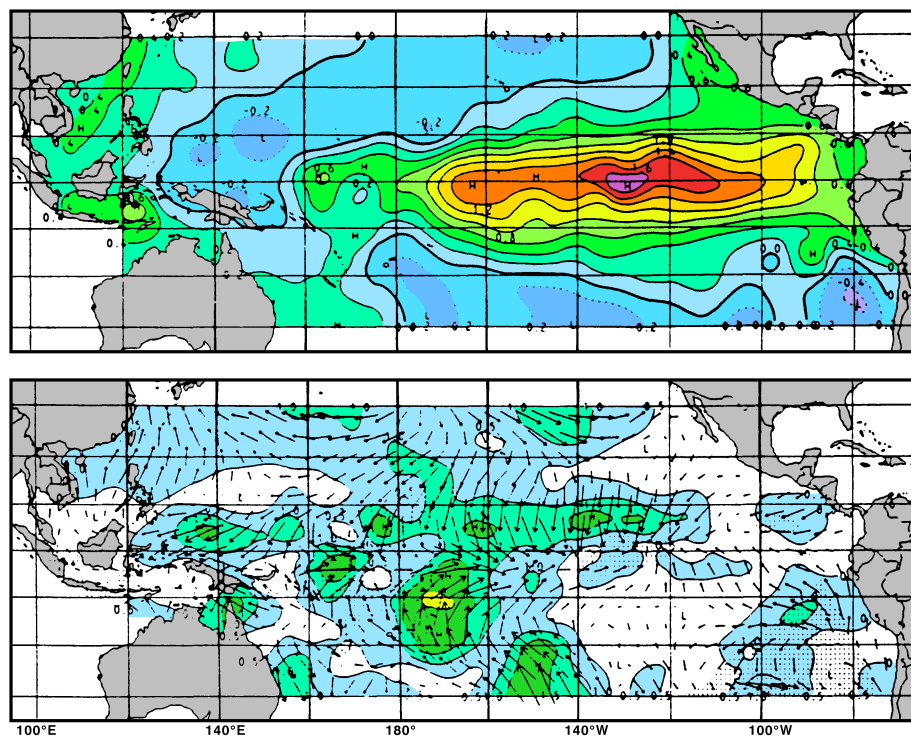


Fig. 19.16. SST anomaly ( $^{\circ}\text{C}$ ) and wind anomaly (m/s), during the mature phase of ENSO (December - February of the year following ENSO). For details see Fig. 19.12. From Rasmusson and Carpenter (1982).

The possibility that ENSO events and other movements of tropical convection systems might be accessible to reliable forecasting one or more seasons in advance has led to new demands on the climate observation network. This need led to the TOGA programme already mentioned earlier, which set itself the goal to "gain a description of the tropical



### Interannual variability of the equatorial Atlantic Ocean

In contrast to the Pacific Ocean, interannual variability in the equatorial Atlantic Ocean is much weaker than its strong seasonal changes. The sea surface temperature along the equator is mainly controlled by advection, and seasonal changes in the current field result in a temperature change of 6 - 8°C at the surface. In comparison, the largest documented interannual temperature change did not exceed 4°C. Nevertheless, when it is recalled that the seasonal upwelling along the coast of Ghana and Ivory Coast is the result of remote wind forcing and Kelvin wave propagation along the equator (Figure 14.20), it is seen that the El Niño mechanism is equally important to the Atlantic as to the Pacific Ocean. It plays a major role in the seasonal behaviour of the tropical ocean, and it appears to be responsible for occasional anomalous warmings of the water along the equator.

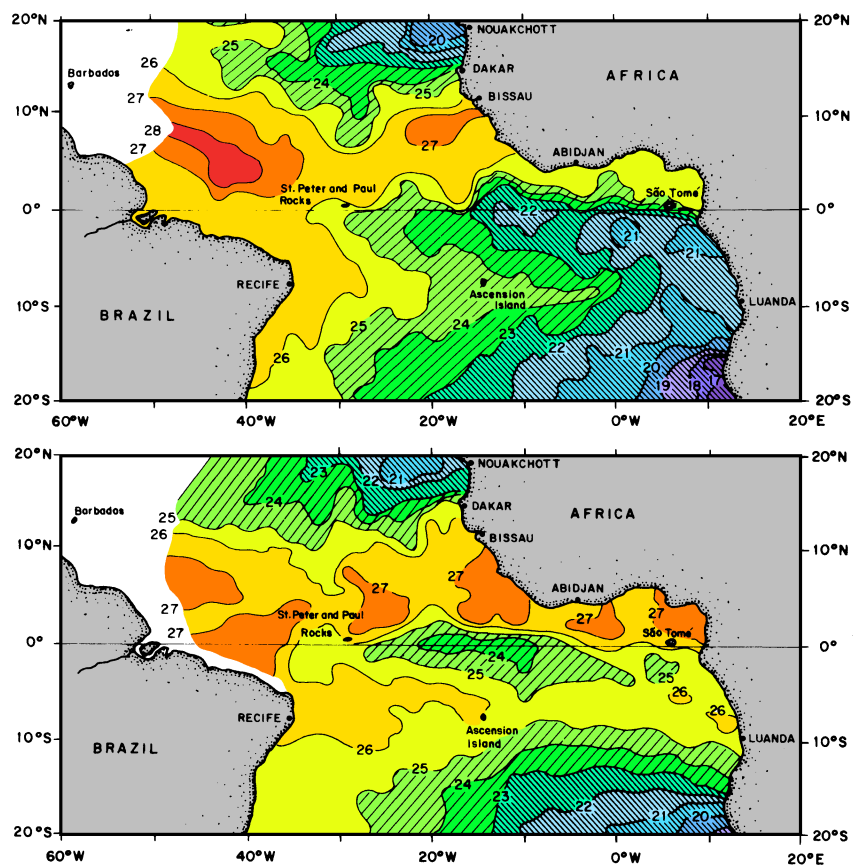


Fig. 19.18. Sea surface temperature (°C) in the tropical Atlantic Ocean. (top) June 1983, (bottom) June 1984. From Philander (1990).



